Farhana Naaz[1], Preeti Lahiri[1*], Chanda Kumari[1], Hemant Kumar Dubey[2]

Spectroscopic, Magnetic and Morphological studies of MgFe₂O₄ Nanopowder

[1]*Department of Chemistry, Institute of Science, MMV, Banaras Hindu University, Varanasi-221005, India plahiri16@yahoo.com*
[2]*Department of Chemistry BRD PG College, Deoria-274001, India*

Spinel type nano ferrite compound $MgFe_2O_4$ was synthesized through sol gel technique using metal nitrates as precursors. The phase composition, morphology and elemental analysis of magnesium ferrite ($MgFe_2O_4$) were performed by X-ray diffraction, fourier transform infrared, atomic force microscopy, energy dispersive x-ray and scanning electron microscopy, analyses.

The sample's X-ray diffraction pattern verifies the existence of single phase material, with the size of its crystallites estimated to be 39.9 nm. Fourier transform infrared examination supported metal-oxygen vibrations corresponding to tetrahedral and octahedral sites, respectively. From scanning electron microscopy image, grain size obtained about 97.7 nm. Raman spectra of the sample shows five Raman active modes ($A_{1g} + E_g + 3F_{2g}$), which is compatible with the spinel structure. Magnetic measurement study at room temperature shows a hysteresis loop behaviour with a low saturation magnetization value, 27.192 emu g^{-1} and a small coercivity value. The optical band gap determined using UV-visible transmittance spectra. Additionally, X-ray photoelectron spectroscopy are used to confirm oxidation states and explore the chemical composition of the sample.

Keywords: Spinel ferrite, Nanocrystalline, X-ray diffraction, Raman spectra, Magnetic properties.

Received 17 January 2023; Accepted 20 June 2023.

Introduction

Ferrites belong to ferromagnetic materials. Ferrite nanomaterials have shown applications in various ways, such as music recording heads, core materials for power transformer in electronics and telecommunications [1,2]. Importantly, magnetic oxide nano-based materials differently from bulk material in terms of their physical, chemical, magnetic and electrical properties [3]. Advantages of nanomaterials rest on their superior thermal stability, environmental and economic advantages to regular counterparts. Owing to their finite size effect, high surface to volume ratio, unique crystal structures, and magnetic characteristics, spinel ferrites nanoparticles have generated a lot of attention in recent years. The general formula for spinel ferrites is AFe_2O_4, where A and Fe are divalent and trivalent metal cations, respectively, with Fe serving as the major constituent. Spinel ferrites are represented by the general formula AFe_2O_4, where A and

Fe are divalent and trivalent metal cations, respectively with Fe as major constituent. Due to their interesting magnetic and electrical properties, they have drawn significant attention to the researchers. Structurally, the spinel ferrite is a cubic closed packed organization of oxygen atoms with 8 formula units per unit cell. Since the radius of oxygen ion is greater than that of metal ion, the oxygen touches each other and form a closed packed Face centered cubic (FCC) lattice. The spreading of cations between A or B site of the lattice depends on both parameters such as preparation routes and heat treatment [4-6].

$MgFe_2O_4$ is the most adaptable, vital and multipurpose spinel ferrites due to unique and reproducible characteristics. They include high saturation magnetization value, and electrical resistivity [7]. Through these magneto-electrical properties $MgFe_2O_4$ show a great utility in the area of catalysis, sensors, high-density recording media and other magnetic technologies [8]. Overall, it is a n-type semiconducting as well as soft

magnetic material. Both photocatalytic activity and catalytic effect of magnesium ferrite in a heterogeneous Fenton-like reaction have been studied [9,10]. Magnesium ferrites typically have the structural formula $(Mg_{1-x}^{2+} Fe_x^{3+})_A[Mg_x^{2+} Fe_{2-x}^{3+}]_B O_4$,is stated as the percentage of the (A) sites occupied by Fe^{3+}cations, where A , B stand for the cationic sites of tetrahedral and octahedral co-ordinations respectively, where x represents the degree of inversion. The structural and magnetic properties of $MgFe_2O_4$ obtained from transmission electron microscopy, XRD, Mossbauer spectroscopy, and magnetometry have been reported [11]. Numerous studies [12,13] on $MgFe_2O_4$ nanoparticles described their nanostructures and many properties, including IR, XRD, SEM, and VSM. N-Suresh kumar [14] synthesized nickel substituted magnesium ferrites by auto combustion method and also studied dielectric and magnetic properties. Magnetic and structural properties of $MgFe_2O_4$ nanopowder synthesized by EDTA-based sol–gel reaction has been reported by Shaban I. Hussein [15]. The electronic structure of $MgFe_2O_4$ nanoparticles created chemically has also been examined by Singh et al [16]. Nanoparticles of $MgFe_2O_4$ have good photoelectrical properties [17]. The synthesis of spinel magnetic oxide involves different chemico-physical approaches that include co-precipitation [18], sol-gel method [19], wet chemical method [20], combustion method [21], hydrothermal method [22], microwave assisted [23], micro-emulsion [24], and ceramic technique [25]. Each method has its own merits and demerits in terms of its ease, efficiency, yield, and costs.

Considering these criteria, we find the sol gel method is effective and can work at low temperatures. Briefly, the sol–gel is a process for developing solid materials from small molecules. In this case, monomers are converted into colloidal solution (sol) that acts as a precursor for an integrated network (or gel) of discrete particles or network polymers. This approach is applicable for the production of metal oxides, like silicon and titanium. Metal alkoxides are common precursors. This chemical technique yields a "sol" which develops into a diphasic system with a liquid phase and solid phase that can have different morphologies, such as discrete particles or continuous polymer networks. Metal alkoxides are typical precursors. Several other names of the sol-gel method are low-temperature self-combustion, auto-ignition, self-propogation, and gel thermal decomposition methods.

We explain, in this paper, the characterization of single phasic cubic spinel ferrites using a sol gel technique by systematic examinations on the structural and physiochemical properties of magnesium ferrites nanoparticles based on several characterization parameter like XRD, SEM, FT-IR, EDX, and magnetic. AFM was utilized to determine the nanoparticles surface roughness and also to obtain 2D and 3D images. Moreover, Raman spectroscopic studies was added to understand the vibrational modes and structural studies of the materials, the optical behaviour of the nano-particles was investigated to determine the absorbance range 300-780 nm, which spans the visible region and is important for various photovoltaic and photocatalytic properties. Moreover, the chemical and elemental state of the nano-particles was concluded by using XPS analysis.

Furthermore, we found that the sol gel technique is the most suitable for creating good molar ratio control with small particle size distribution due to molecular-level mixing, fast processing time, lower temperatures and inexpensive.

I. Experimental Procedure

$MgFe_2O_4$ was prepared via the auto-combustion aided sol-gel method. The energy required to produce the ferrite nano-particles is provided in this procedure by a redox process using a thermal precursor and citric acid as a fuel [26]. Metal nitrates were served as a source of soluble cations and the oxidant [27]. Citric acid ($C_6H_8O_7$) was employed as both a fuel and a chelating agent, forming interactions with metal ions and preventing the precipitation of hydroxilated compounds [28]. Analytical reagent grade, Merck India, used in this work were: iron nitrate ($Fe(NO_3)_3 \cdot 9H_2O$, 99%) magnesium nitrate ($Mg(NO_3)_2 \cdot 6H_2O$, 98%) and citric acid ($C_6H_8O_7$). The desired composition was obtained by taking stoichiometric molar ratio (2:1) of $Fe(NO_3)_3.9H_2O$ (0.032 mol) and $Mg(NO_3)_2.6H_2O$ (0.016 mol) dissolved in 20 ml of double distilled water. To promote homogeneity, an equimolar amount of citric acid (0.046 mol) was added to an aqueous mixture, which was magnetically agitated while the reaction temperature was kept at 60^0C.The pH was optimize to 7.0 by adding ammonia solution drop by drop under steady stirring until the mixture was neutralised and turned into sol. The sol developed into a black gel after 8 hours of stirring, releasing a huge amount of gases (CO_2, H_2O, N_2) in the process. The gel was dried for 12 hours at 100 ^0C, with its volume swelling by nearly five times, yielding a fluffy, abundant powder. At end, the dried gel was grounded and annealed at 500 ^0C for 3 h to get a dark brown ferrite nanoparticle as a final product. The Flow chart of the sol-gel synthesis process of $MgFe_2O_4$ nanoparticles is given below.

The structural investigations (crystal structure and phase analysis) of the synthesized nanomaterial were performed by using XRD, Rigaku Miniflex 600, Japan technique with Cu-Kα radiation (λ=1.5406 A^0) within 2θ range 20-80º. The FTIR spectrum was obtained in the range 400 cm^{-1} to 4000 cm^{-1} employing a FTIR spectrometer, Perkin Elmer. SEM, (ZEISS model EVO-18 research, Germany) and AFM, model NTEGRA PRIMA, NT-MDT, Russia was used to determine microstructure and surface roughness of nanomaterial respectively. The quantitative elemental analysis was carried out by means of EDAX analyser (EDX, Oxford instrument USA). The magnetic behaviour of the produced sample was investigated using a SQUID-based magnetometer (MPMS 3) in the magnetic field range of 20 kOe. Raman spectra was recorded to estimate the frequency mode of tetrahedral and octahedral sites of cubic spinel at frequency range of 100-800 cm^{-1}, using the model RENISHAW In-VIA Raman microscope. UV–VIS diffuse reflectance spectra were acquired by UV-VIS Spectrophotometer SHIMADZU in the wavelength range of 200–600 nm (UV-1700 Pharma Spec), chemical and elemental state analysis of the investigated surface were indicated by XPS, Thermo scientific K-ALFHA Surface Analysis.

Farhana Naaz, Preeti Lahiri, Chanda Kumari, Hemant Kumar Dubey
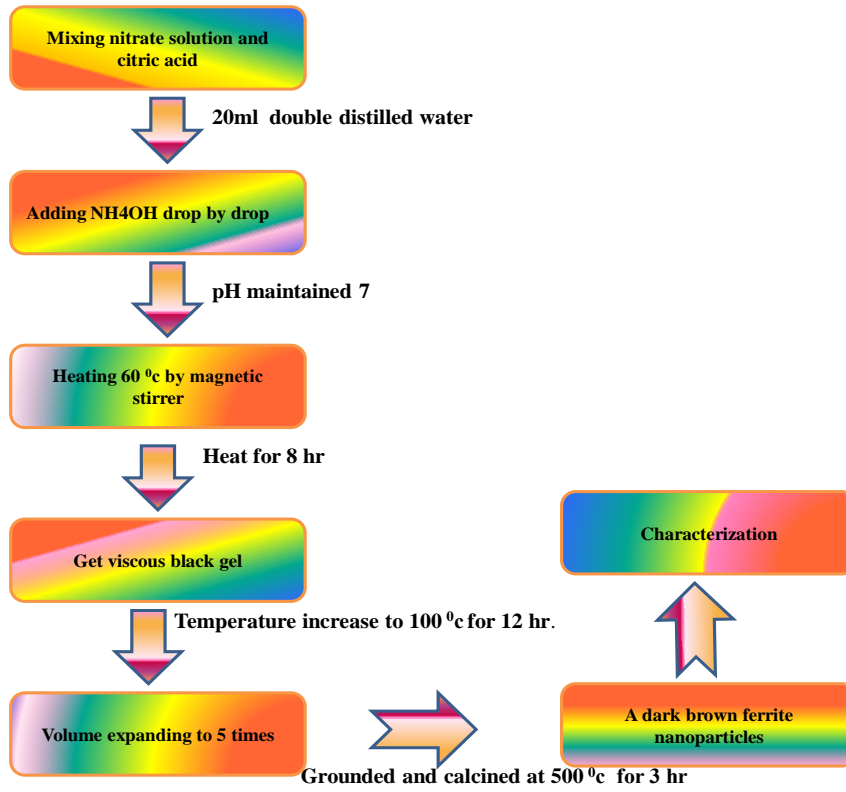
Flow chart of the sol-gel synthesis process of MgFe$_2$O$_4$ nanoparticles.

II. Results and Discussion

2.1 FTIR analysis

Figure 1 illustrates room temperature IR spectrum of the magnesium ferrite sample determined in the range 400 to 4000 cm^{-1}. The calcined MgFe$_2$O$_4$ magnetic nanoparticle exhibits two main absorption bands at around 630 and 441 cm^{-1}. The higher frequency band (ν_1) and the lower frequency band (ν_2), specify the metal-oxygen intrinsic stretching vibration of the spinel unit cell in the tetrahedral (A) and octahedral (B) sites [29] respectively. The observed variance in band positions is due to the distance between the metal-oxygen ions connected to the octahedral and tetrahedral complexes. This indicates bond formation and the phase stability of synthesized material. TheFTIR results confirmed that the sample has spinel structure of MgFe$_2$O$_4$, which was revealed by the XRD results. The strong signature band observed at 3420 cm^{-1} is assigned to the symmetric streching vibrations of O-H groups [30]. The symmetric stretching vibration of hydrogen bonded water molecules is responsible for the perturbations in the absorption band between 1030 and 1630 cm^{-1}, indicating the existence of absorbed or free water molecules in a sample. The force constant (k) was evaluated from the equation [31],

$$k = 4\pi^2 c^2 m \nu^2 \qquad (1)$$

where, c is the velocity of light (2.99×10^8 m/sec), v is the vibrational frequency of the A and B sites, m is the reduced mass for the metal-oxygen ions. Values obtained for force constant are shown in Table 1.
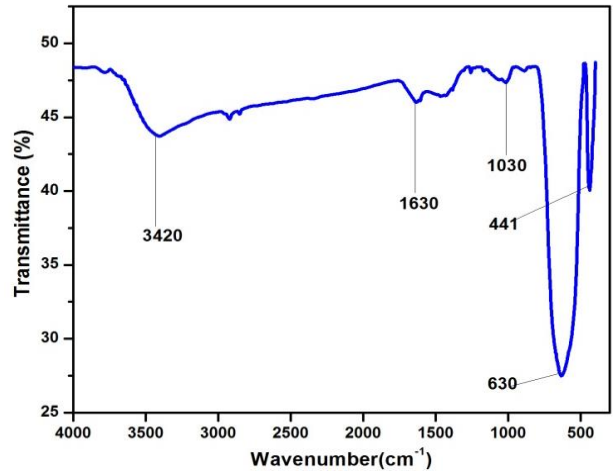
Fig. 1. The FT-IR spectra of Magnesium ferrite nanoparticles.

2.2 X-ray diffraction analysis

Powder X–ray diffraction studies are helpful in determining the structure and particle size of nanoparticles produced. The XRD of powdered sample of MgFe$_2$O$_4$ obtained by sol-gel method is illustrated in Fig. 2. The XRD pattern reveals formation of monophase face centered cubic (fcc) spinel structure. All Bragg reflections have been indexed as (111), (220), (311), (222), (400), (422), (511) and (440). All observed sharp diffraction peaks were compared with magnesium ferrite JCPDS card number 89-3084. The most intense peak at 2θ=35.55 degree corresponds to crystalline plane of

magnesium ferrite which indicates a fine particle nature of the particles.
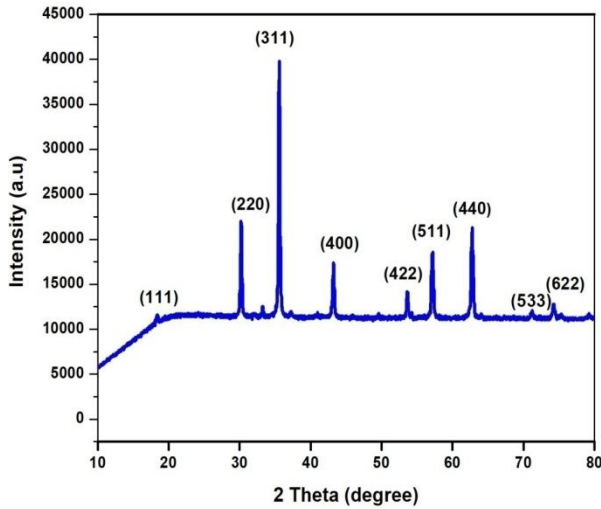
Fig. 2. X-ray diffraction patterns of Magnesium ferrites nanoparticles.

The average crystallite size (D) was estimated from the XRD peak broadening of the most intense peak (311) using the Scherrer's relation [32],

$$D = \frac{k\lambda}{\beta \cos \theta} \qquad (2)$$

where, k is Scherrer's constant (0.91), λ is wavelength (λ=1.5406 A^0). The parameters D and θ are taken as crystallite size and Bragg's angle respectively. Here β is the full width at half maxima (FWHM) of XRD peaks. Table 1 shows the calculated values for crystallite size, x-ray density, lattice constant, and cell volume based on x-ray data. The average crystallite size (D) of the synthesized material was found to be 39.9 nm (Table I) for MgFe$_2$O$_4$. The lower value (36.6 nm) was reported for the same sample synthesized by co-precipitation method [33].

The lattice constant 'a' was calculated for prominent (311) peak using the following relation,

$$a = d\sqrt{h^2 + k^2 + l^2} \qquad (3)$$

where d is interplanar distance and *h,k,l* are the miller indices of the diffraction plane. The calculated lattice parameter 'a' (8.35 A^0) for MgFe$_2$O$_4$ agrees well with the reported value of 8.37A^0 [34]. Following relation was used to calculate x-ray(ρ_x) density,

$$\rho_x = ZM/N_A a^3 \qquad (4)$$

where Z is the number of molecules per unit cell (Z = 8), M is the molecular mass of the sample, and N is the Avogadro's number (N$_A$ = 6.026 × 10^{23} atoms mol^{-1}). The sample of ferrite was determined to have a density of 4.554 g/cm^3 (Table 1).

Utilizing the following formula, the volume of the unit cell was computed,

$$V = a^3 \qquad (5)$$

in(A^0)^3 units. Relationships were used to determine the distance between magnetic ions and the hopping length (L) in the A sites (tetrahedral) and B sites (octahedral) [35],

$$L_A = \frac{a\sqrt{3}}{4} \text{ and } L_B = \frac{a\sqrt{2}}{4} \qquad (6)$$

It was observed that the hopping lengths for two sites were 3.615 A^0 and 2.951 A^0 respectively in Table 1.

2.3 SEM and EDX analysis

The surface morphologies and elemental composition of magnesium ferrite nano powder were examined by SEM, coupled with EDX analysis. In Fig. 3 (a) SEM image of calcined MgFe$_2$O$_4$ sample is illustrated. Agglomerates and non-uniformity are evident in the sample. The grain size was estimated using AIL [36]. The number of grain boundaries intersected by a randomly chosen straight line of length L drawn on micrographs was counted, and the average grain diameter (G), which is around 98 nm, was computed, N is the total number of the complete sample, and M is the magnification.

$$G = 1.5L/MN \qquad (7)$$

The elemental analysis of the prepared MgFe$_2$O$_4$ nano powder was obtained by EDX analysis and weight % and atomic % of elements were shown in the Table 2. The estimated ferrite composition is confirmed by EDX data, which is reinforced by the good agreement between experimental and theoretical Mg/Fe molar ratio (Table 2). The sample's EDX pattern, which displays the presence of Mg, Fe, and O without precipitating cations, is demonstrated in Fig. 3(b).

Table 1.

Some structural parameters; crystalline size, lattice parameter, X-ray density, unit cell volume, hopping length for A-Site (d$_A$) and B-Site (d$_B$) and force constants for octahedral (k$_o$) and tetrahedral (k$_t$) sites of Magnesium ferrite nanoparticles

Sample	Crystalline size (nm)	Lattice parameter (A^0)	X-ray density (g/cc)	Unit cell volume (A^0)^3	Force constant k$_o$×10^5 (dyne/cm)	Force constant k$_t$×10^5 (dyne/cm)	A site d$_A$ (A.u)	B Site d$_B$ (A.u)
MgFe$_2$O$_4$	39.9	8.35	4.554	583.79	1.414	2.886	3.615	2.951

Farhana Naaz, Preeti Lahiri, Chanda Kumari, Hemant Kumar Dubey
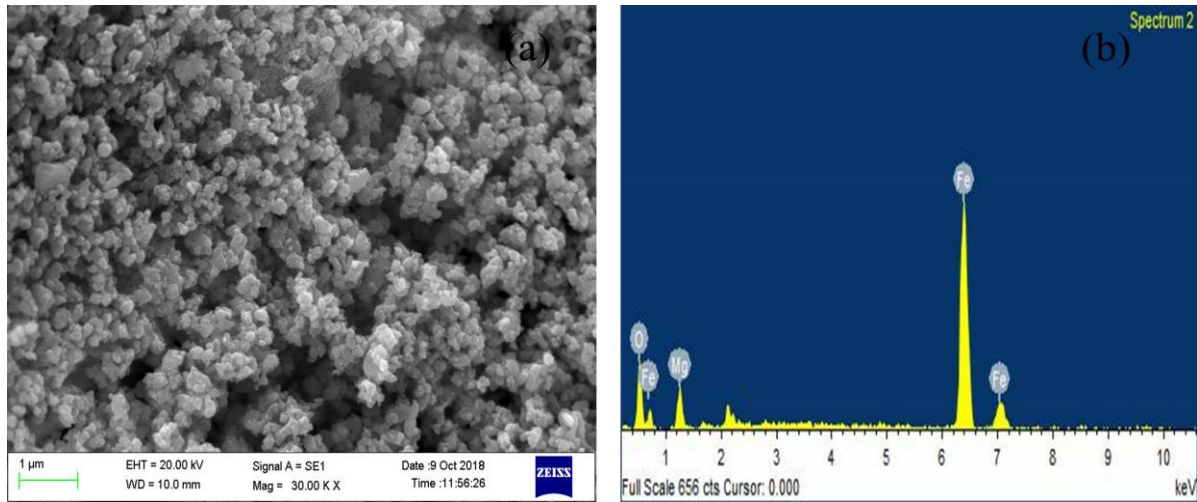
Fig. 3. (a) SEM image and (b) EDX analysis of Magnesium ferrite nanoparticles.

Table 2.

The observed and theoretical elemental composition value of $MgFe_2O_4$ obtained from EDX analysis

Element	Experimental value		Theoretical value	
	Weight %	Atomic %	Weight %	Atomic %
O	21.51	44.41	31.98	57.15
Mg	11.95	16.23	12.15	14.26
Fe	66.54	39.35	55.84	28.57
TOTAL	100.0			

2.4 AFM analysis

Thin film topography of $MgFe_2O_4$ nanoparticles obtained by AFM (atomic force microscopy). This microscopic technique has several advantages for characterising nanoparticle. Images obtained via AFM display data in two and three dimensions, allowing for the quantitative generation of information on both individual particles and groups of particles. Fig. 4. display the 2D and 3D AFM images of $MgFe_2O_4$ respectively and its related histogram and size distribution. The average roughness (Rq) and root mean square roughness (RMS) values obtained about 5.982 nm and 7.541 nm respectively. Also, the maximum height (R_p) and a maximum depth (R_v) observed as 35.645 nm and 27.449 nm respectively.

2.5 Raman analysis

Raman spectroscopic technique is a powerful technique to identify the structural and vibrational properties of the material $MgFe_2O_4$ spinel. $MgFe_2O_4$ crystallises as an AB_2O_4 type spinel structure with eight formula units per unit cell in Fd3m space group. According to results from group theoretical calculations, AFe_2O_4 type spinel structures consist of five raman active phonon modes, namely $A_{1g}+E_g+3F_{2g}$, which are made up of the motion of O ions and both A and B site ions [37,38]. Figure 5 displays the $MgFe_2O_4$ sample's raman spectra in the frequency range of 100–800 cm^{-1}. In Table 3 and Fig. 5, several peaks have been identified. The A_{1g} (1) mode is caused by the symmetric stretching of oxygen atoms along Fe–O (or M–O) tetrahedral bonds. The E_g & $F_{2g}(3)$ modes are caused by the symmetric and asymmetric bending of oxygen with respect to Fe respectively. The F_{2g} (2) mode is caused by the asymmetric stretching of the Fe–O bond,

F_{2g} (1) is due to translational movement of the whole tetrahedron (FeO$_4$) [39], while $F_{2g}(2)$ and $F_{2g}(3)$ related to the vibrations of octahedral group.

Table 3.

Raman modes of spinel $MgFe_2O_4$ and their assignments

Raman Modes (cm^{-1})	Assignment
209	$F_{2g}(1)$
330	E_g
479	$F_{2g}(2)$
549	$F_{2g}(3)$
707	A_{1g}

In our system, $MgFe_2O_4$ nanopowder contains five peaks at 209, 330, 479, 549 and 707 cm^{-1} (Table 3). These bands are given the following designations: $F_{2g}(1)$, E_g, F_{2g} (2), F_{2g} (3) and A_{1g} (1) correspondingly. These modes match the reported [40] values of 217, 333, 486, 554, and 715 cm^{-1} for magnesium ferrites. It agrees well with the current strong band location for $MgFe_2O_4$ at 707 cm^{-1}, which J. Chandradass [41] attributed to the A_{1g} mode in $MgFe_2O_4$.

2.6 VSM analysis

To investigate the magnetic behaviour of spinel $MgFe_2O_4$, SQUID based magnetometer has been employed under magnetic field upto 20 kOe. By applying a magnetic field to a material that becomes magnetized by the magnetic field, the M-H loop or hysteresis curve is
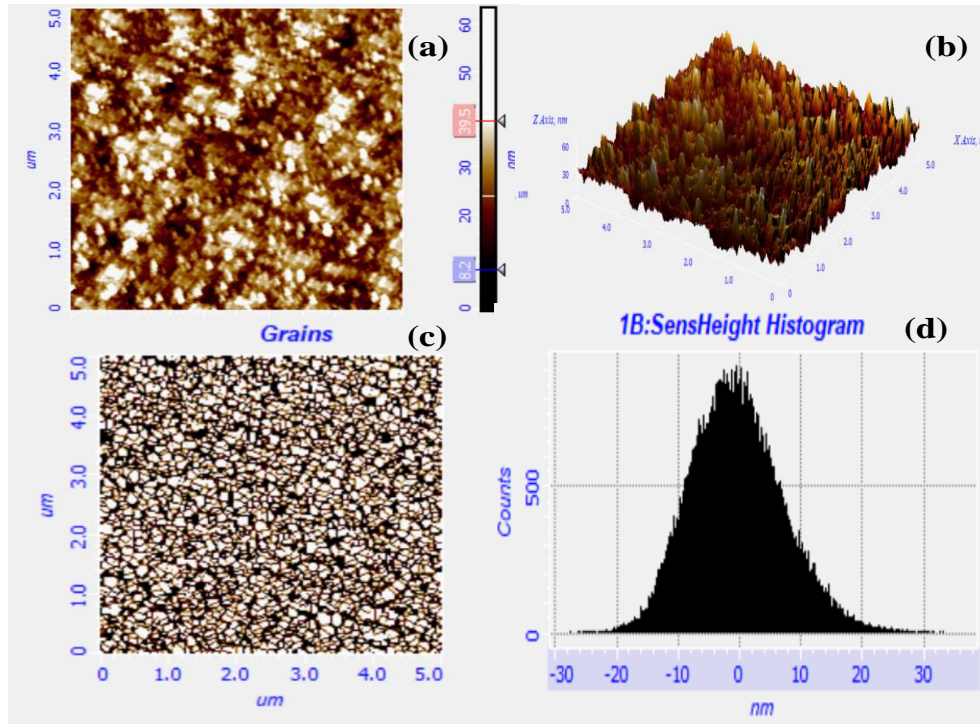
Fig. 4. AFM images of MgFe$_2$O$_4$ nanoparticles. (a) Two dimension (2D) (b) Three dimension (3D) (c) examination of grain size (d) histogram of MgFe$_2$O$_4$ nanoparticles.
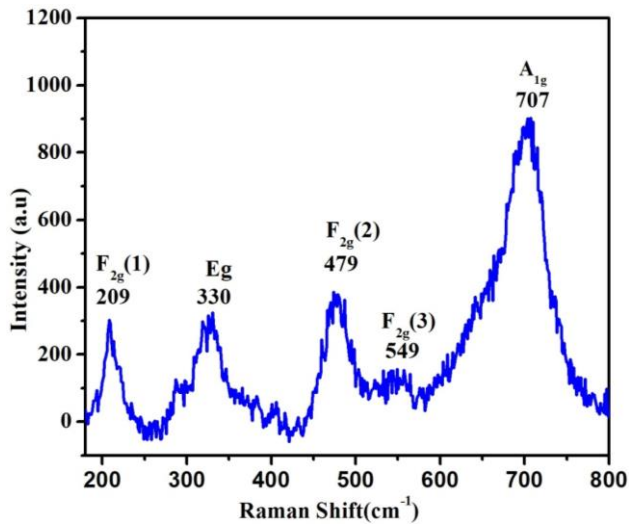
Fig. 5. Raman spectra of synthesized spinel MgFe$_2$O$_4$ nanoparticles.
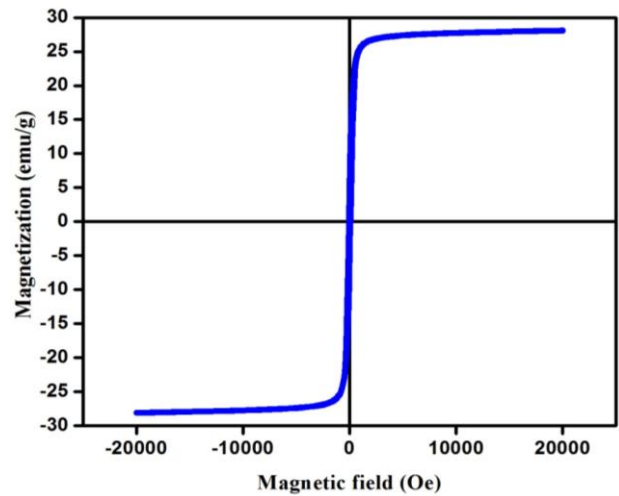
Fig. 6. Magnetisation curve of MgFe$_2$O$_4$ nanopowder under applied magnetic field of 20 kOe.

formed. Remanence magnetization is the value of magnetization at which field is zero. The point on the curve where the magnetization is zero and the field is negative is referred to as the coercive field, and the saturation magnetization is the point at which the magnetising force stops increasing the magnetic induction in a magnetic material. The room temperature magnetization curve of the calcined MgFe$_2$O$_4$ nanoparticle

obtained from M-H loop is depicted in Fig. 6. This curve denotes hysteresis ferromagnetism and is typical for soft magnetic materials.

Magnetic parameters such as saturation magnetization (M_s), coercivity (H_c), retaintivity (M_r) and remanent ratio (R) values; 27.192 emu g^{-1}, 36.0 Oe, 0.4646 emu g^{-1}, 0.0170 respectively of ferrite nanoparticles are listed in Table 4. It was observed that the saturation value of

Table 4.

The coercivity (H_c), saturation magnetization (M_s), retaintivity (M_r), remanant ratio (R), and magnetic moment (μ_B) obtained at a magnetic field at 20 k Oe at room temperature

Sample	M_s (emu/g)	H_c (Oe)	M_r (emu/g)	M_r/M μ_B
MgFe$_2$O$_4$	27.192	36.00	0.4646	0.0170 0.9737

Farhana Naaz, Preeti Lahiri, Chanda Kumari, Hemant Kumar Dubey

27.192 emu/g obtained in the sample calcined at 500^0C (crystallite size of 39.9 nm) is close to the values of 33.4 emu g^{-1} for bulk $MgFe_2O_4$ [42] and 30.6 emu g^{-1} for sol-gel/combustion synthesized $MgFe_2O_4$ (crystallite size of 78 nm) [43], while it is higher than the values of 14.09 emu g^{-1} for co-precipitation synthesized $MgFe_2O_4$ nanoparticles (diameters of 34.4 nm) [44]. Remanent magnetisation (M_r) value for the sample was obtained from the Fig. 6. The $MgFe_2O_4$ nanopowder's Mr/Ms ratio, which measures remanent magnetization to bulk saturation magnetization, was calculated to be 0.0170. A significant portion of superparamagnetic particles are indicated by the low Mr/Ms value. The coercivity (H_c) was found to be 36 Oe (Table 4) for the $MgFe_2O_4$ nanaparticle. The value is less than the value of 165 Oe for $MgFe_2O_4$ produced by sol–gel/combustion but is comparable to the value of 48.86 Oe for nanoparticles made by coprecipitation.

Sub-lattices A and B are magnetised in opposing directions by the spins of the A and B site ions, producing a magnetic moment that is equal to the difference between the magnetic moments of the A and B site ions [45]. The magnetic moment per formula unit is given by the equation,

$$M = M_B - M_A \qquad (8)$$

where M_B and M_A stand for the B- and A- sublattice magnetic moments in uB, respectively. This formula is based on Neel's two sub-lattice model of ferrimagnetism [46]. The Ms value is typically determined by the net magnetic moment. According to the literatures [47,48], the octahedral positions are preferentially occupied by Mg^{2+} cations in the bulk magnesium ferrite, which has an inverted spinel structure. The cationic distribution on tetrahedral and octahedral lattice sites has a significant impact on the Ms of spinel ferrite nanoparticles [49].

The following relation [50] was used to compute the magnetic moment per formula unit in Bohr magneton (B) of the sample,

$$\mu_B = M_w \times M_s / 5585 \qquad (9)$$

where M_S is the saturation magnetization in the electromagnetic unit and M_w is sample's molecular weight. Table 4 displayed the magnetic moment's value.

2.7 Optical studies

The UV-vis spectra of $MgFe_2O_4$ were conducted using dil HCl as a solvent in order to examine the optical characteristics of the prepared nanoparticles. The absorbance extends around 300-600 nm shows visible region which is important for numerous application in photo-catalytic and photo voltaic activity. Fig. 7(a) displays the UV-visible absorbtion spectra of 500°C-calcined magnesium ferrite nanopowder as a function of wavelength (nm). Typical band throughout 300-500 nm is proclaimed in optical absorption spectra of $MgFe_2O_4$ nanoparticles. These bands results from octahedral coordination of Fe^{3+} ions [51]. The absorption cutoff wavelength is 427.5 nm. The optical band gap energy (Eg) of magnetic nanoparticles sample was calculated according to the Tauc relationship as given below [52],

$$Ahv = A(hv − Eg)^n \qquad (10)$$

where (α) absorption coefficient, (Eg) the energy gap, (A) is constant for different transition, (h) is Plank constant ($6.62.10^{-34}$ J s^{-1}photon $^{-1}$), (hv) are the energy of photon and the value of n is either ½ for indirect band gap or 2 for direct band gap. The intercept on the (hv) axis can be found by projecting the plot to the point where $(\alpha hv)^2 = 0$ as shown in Fig. 7(b). The intercept of the straight line at α=0 was used to calculate the band gap energy, which was found to be 2.91eV, somewhat higher than the stated value range of 2.0-2.2 [53,54].
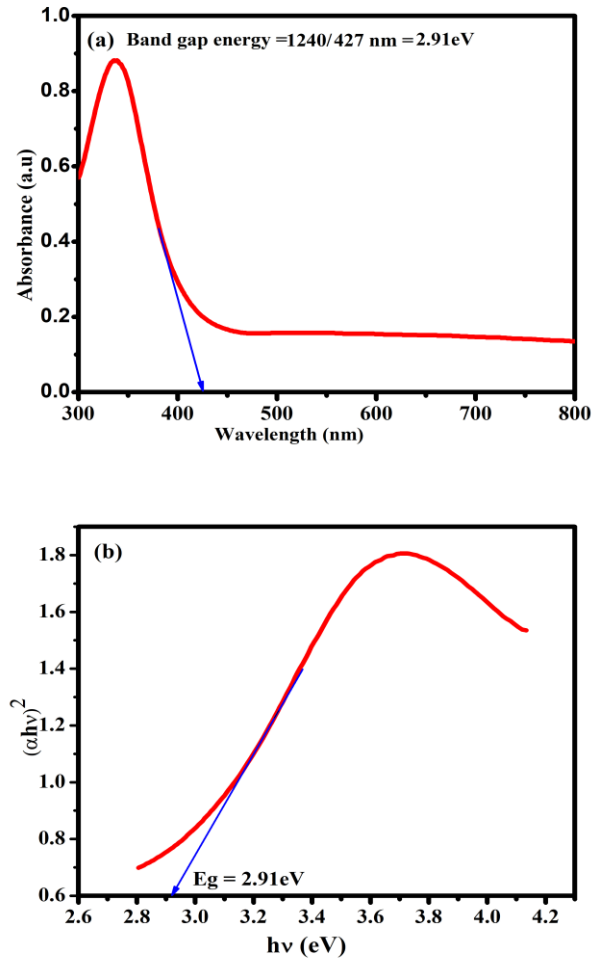
Fig. 7. (a) UV visible absorbtion spectra of the $MgFe_2O_4$. (b) $(\alpha hv)^2$ [$eVcm^{-1}$]^2 versus photon energy (hv) graphs for $MgFe_2O_4$.

2.8 XPS analysis

XPS is used to study the chemical and elemental state analysis at the depth of about 5-10 nm of the investigated surface of the sample. XPS is that technique which not only shows elements are present but also what other elements they are bounded to. Also it examined the energy of the component.

XPS spectrum displayed in Fig. 8, the spectrum reveals chemical composition of the sample $MgFe_2O_4$ nanoparticles attributed to element Mg, Fe, O and unintentional element like carbon. As shown in Fig. 8 (a) two characteristic peaks at 724.88 eV and 711.28 eV indicated as binding energy which corresponds to $Fe^{3+}2p_{1/2}$ and Fe^{2+} $2p_{3/2}$ orbital which is similar to the
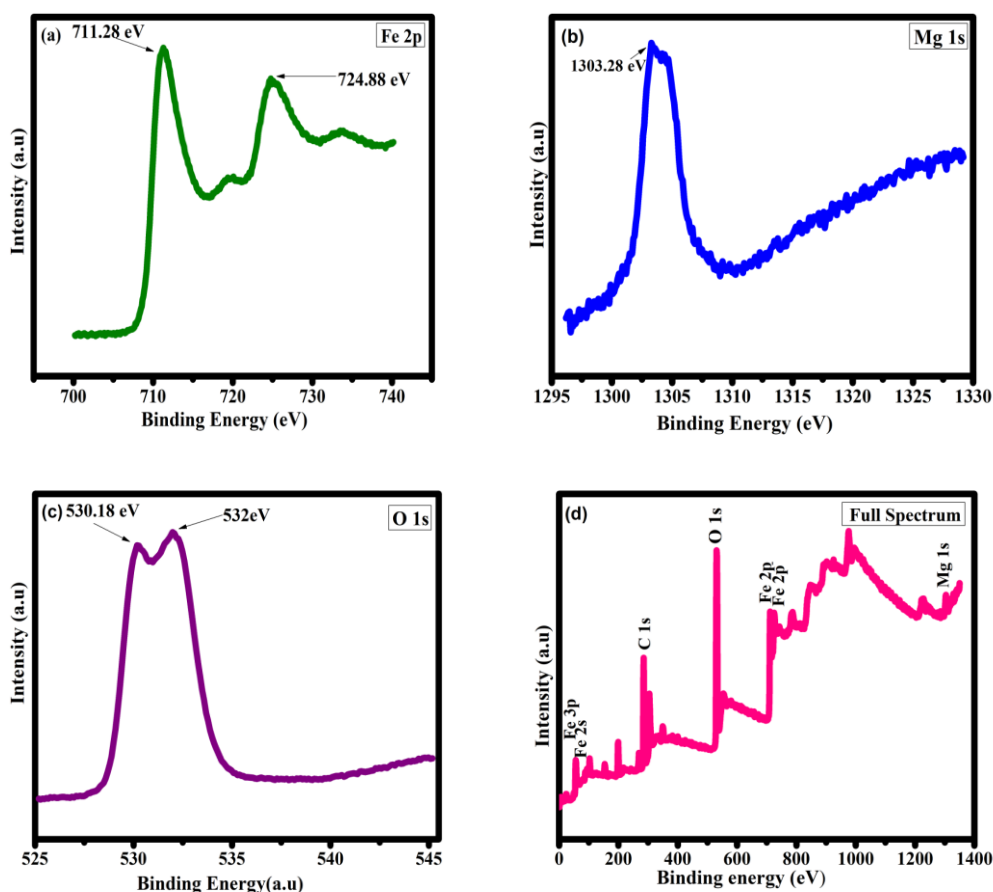
Fig. 8. XPS spectra of $MgFe_2O_4$ nanoparticles (a) Fe 2p (b) Mg 1s (c) O 1s (d) Full spectrum.

reported earlier by Hengli Xiang [55]. The single peak located at 1303.28 eV would be attributed to Mg 1s which reveal the oxidation state Mg^{+2} in the sample which is shown in Fig. 8 (b)that is in fine agreement with some earlier results [56].The peak located at 530.18 eV is attributed to O 1s region which appears due to metal-oxygen bonding and the peak at 532.00 eV as shown in Fig. 8 (c) represents oxygen vacancies or metal hydroxyl bonds at the surface, full spectrum of the sample are shown in Fig. 8d. Table 5 shows the elements and its peak position of Fe 2p, O 1s, Mg 2p of the sample.

Table 5.

Peak position in (eV) of Fe2p, O1s, Mg2p, spectra of $MgFe_2O_4$ nanoparticles.

Peak	Peak position (eV)
Fe 2p	724.88
	711.28
O 1s	530.18
	532.00
Mg 2p	1303.28

Conclusions

In this study, we present evidence that sol-gel-produced magnesium ferrites nanoparticles can form a single-phase cubic spinel structure. Surface morphology image illustrated with some agglomerated size particles. The synthesized composition's Mg, Fe, and O content are confirmed by the EDX analysis spectrum. Five Raman active modes E_g, $3F_{2g}$, A_{1g} in the range of 209-707 cm^{-1}, which are anticipated in the spinel structure, were validated by a Raman investigation. Raman study confirmed the existence of five Raman active modes E_g, $3F_{2g}$, A_{1g} in the range of 209-707 cm^{-1} which are predictable in the spinel structure. Magnetic measurement shows soft magnetic behaviour of the sample with the M_s value 27.129 emu/g. AFM is utilized to estimate the height, grain size, and average roughness of the particles. The band gap energy at 2.91eV are obtained by UV-VIS absorbance spectra while chemical composition and elemental states are determined by X-ray photoelectron spectroscopy (XPS).

Conflicts of Interest

There are no conflicts of interest, according to the authors.

Farhana Naaz – M.Sc, Research Scholar;
*Preeti La*hiri – Ph.D., Professor;
Chanda Kumari – Ph.D., Senior Research Scholar;
Hemant Kumar Dubey – Ph.D., Assistant Professor.

[1]   1. J. D Adam, L. E Davis, G. F.Dionne, E. F Schloemann, S. N. Stitzer, *Ferrite Devices and Materials*,IEEE Transactions on Microwave Theory and Techniques, 50, 721 (2002); https://doi.org/10.1109/22.989957.

[2]   V.G. Harris,A. Geiler, Y. Chen, S.D. Yoon, W. Mingzhong, A. Yang, Z. Chen, H. Peng, V. Patanjali, X. Zuo, Parimi,ManasoriAbe, O. Acher and C.Vittoria, *Recent advances in processing and applications of microwave Ferrites*, Journal of Magnetism and Magnetic Materials, 321, 2035 (2009); https://doi.org/10.1016/j.jmmm.2009.01.004.

[3]   J. Balavijayalakshmi and Greeshma, *Synthesis and Characterization of Magnesium ferrite nanoparticles by Co-precipitation method*, Journal Environ. Nanotechnology, 2, 53 (2013), https://doi.org/10.13074/jent.2013.06.132015.

[4]   V.B. Kawade, G.K. Bichile and K.M. Jadhav, *X-ray and infrared studies of chromium substituted magnesium*,Material Letters 42, 33 (2000);https://doi.org/10.1016/S0167-577X(99)00155-X.

[5]   C.J. Kriessman and S.E. Harrison, *Cation Distributions in Ferrospinels Magnesium-Manganese Ferrites*, Physical Review, 103, 1 (1956); https://doi.org/10.1103/PhysRev.103.857.

[6]   E.W. Gorter. *Magnetization in Ferrites: Saturation Magnetization of Ferrites with Spinel Structure*, Nature, 165, 78 (1950); https://doi.org/10.1038/165798a0.

[7]   S.K. Pradhan, S. Bid, M. Gateshki and V. Petkov, *Microstructure characterization and cation distribution nanocrystalline magnesium ferrite prepared by ball milling*, Material Chemistry Physics, 93, 224 (2005); https://doi.org/10.1016/j.matchemphys.2005.03.017.

[8]   R.J. Willey, P. Noirclerc and G. Busca, *Preparation and characteriation of magnesium chromite and magnesium aerogels*. Chemical Engineering Communication, 123, 1 (2013); https://doi.org/10.1080/00986449308936161.

[9]   R. Dom , R. Subasri, K. Radha and P.H. Borse, *Synthesis of solar active nanocrystalline ferrite, MFe2O4 (M: Ca, Zn, Mg) photocatalyst by microwave irradiation*, Solid. State communication, 151, 470-473, (2011); https://doi.org/10.1016/j.ssc.2010.12.034.

[10] C. Xiong, Q. Chen, W. Lu, H. Gao, W. Lu and Z. Gao, *Novel Fe-based complex oxide catalysts for Hydroxylation of phenol*, Catalysis Letters, 69, 231 (2000); https://doi.org/ 10.1023/A:1019042527870.

[11] S.A. Oliver, R. J. Willey, H.H. Hamdeh,G. Oliveri ,G. Busca, *Structure and magnetic properties of magnesium ferrite fine powder,* Scripta Metallurgica et Materialia, 33, 1695 (1995); https://doi.org/10.1016/0956-716X(95)00412-O.

[12] R. Paulsingh and C. Venkataraju, *Effect of calcinations on the structural and magnetic properties of magnesium ferrite nanoparticles prepared by sol gel method,* Chinese Journal Physics, 56, 2218 (2018);https://doi.org/10.1016/j.cjph.2018.07.005.

[13] A.Tariq , U. Ullah, I. Ahmad, M. Asif, I. Sadiq, H. *Haleem.Comparative analysis of the Magnesium Ferrite (MgFe₂O₄) nanoparticles synthesized by three different routes*. IET Nanobiotechnology, 137, 697 (2019); https://doi.org/10.1049/iet-nbt.2018.5032.

[14] N.S Kumar, N. Das, K. Devlal, S. Seema, M.S. Shekhawat, M. Hidayath and A.S. Khader,*Dielectric and Magnetic Studies of Ni-Mg Mixed ferrites by combustion Method,AIP Conference Proceeding*, 2220, 1 (2020);https://doi.org/10.1063/5.0001907.

[15] S.I. Hussein, A.S. Elkady, M.M. Rashad, A.G. Mostafa and R.M. Megahid, *Structural and magnetic properties of magnesium ferrite nanoparticles prepared via EDTA-based sol–gel reaction*, Journal of Magnetism and Magnetic Materials, 379, 9 (2015); https://doi.org/10.1016/j.jmmm.2014.11.079.

[16] 16. J.P. Singh, S.O. Won, W.C. Lim, I.J. Lee and K.H. Chae, *Electronic structure studies of chemically synthesized MgFe₂O₄ nanoparticles*, Journal Molecular Structures 1108, 444 (2016); https://doi.org/10.1016/j.molstruc.2015.12.002.

[17] Y. He, X. Yang, J. Lin, Q. Lin and J. Dong. *Mössbauer Spectroscopy, Structural and Magnetic Studies of Zn2+ Substituted Magnesium Ferrite Nanomaterials Prepared by Sol-Gel Method*, Journal Nanomaterials, 1, 1 (2015); http://dx.doi.org/10.1155/2015/854840.

[18] S. Thankachan, S. Xavier, B. Jacob and E.M. Mohammed, *A comparative study of structural electrical and magnetic properties of magnesium ferrite nanoparticles synthesised by solgel and co- precipitation techniques*.J. Exper. Nanosc. 8, 347 (2013); https://doi.org/10.1080/17458080.2012.690892.

[19] R.P. Singh and Venkataraju, *Effect of calcinations on the structural and magnetic properties of magnesium ferrite prepared by sol gel method*, Chinese. J. Phys. 56, 2218 (2018); https://doi.org/10.1016/j.cjph.2018.07.005.

[20] M. Kurain, S. Thankachan, D.S. Nair, E.K. Aswathy, A. BABU, A. Thomas and B.K Krisjna, *Structural, magnetic, and acidic properties of cobalt ferrite nanoparticles synthesised by wet chemical methods*, Journal Advance Ceramic, 4, 199 (2015); https://doi.org/10.1007/s40145-015-0149-x.

[21] S. Hasan, B. Azhdar, *Facile synthesis of nanocrystalline zinc ferrite via a self propagatin combustion method* Material Letters, 61, 347 (2007)*;* https://doi.org/10.1016/j.matlet.2006.04.06.

[22] S.Verma, P.A. Joy, Y.B. Khollam, H.S. Potdar and S.B. Deshpande, *Synthesis of nanosized MgFe2O4 powders by microwave hydrothermal method*, Material Letters58, 1092, (2004);https://doi.org/10.1016/j.matlet.2003.08.025.

[23]   K.K. Zeynep, R. Boncukcuoglu, I.H. Karakas and M. Ertugru, *The effects of heat treatment on the synthesis of nickel ferrite (NiFe2O4) nanoparticles using the microwave assisted combustion method*,Journal of Magnetism and Magnetic Materials, 298-306, (2015); https://doi.org/10.1016/j.jmmm.2014.08.045.

[24]   P. Holec, J. Plocek, D. Niznansky, Poltierova and J. Vejpravova. *Preparation of MgFe2O4 nanoparticles by microemulsion method, J. Sol-Gel*, ScienceTechnology, 51, 301 (2009); https://doi.org/10.1007/s10971-009-1962-x.

[25]   La Agusu, Alimin, L. O. Ahmad, M. Z. Firihu, S. Mitsudo, H. Kikuchi, *Crystal and microstructure of MnFe2O4 synthesized by ceramic method using manganese ore and iron sand as raw materials*, Journal Physics Conference, 1153, 1 (2019); https://doi.org/10.1088/1742-6596/1153/1/012056.

[26]   S. S. Jagtap, M.R. Sopan. *Synthesis and characterization of Mg-Ni ferrite prepared by Sol gel autocumbustion method*, Appl. Res. Devl. Inst. J. 8, 1, (2013);

[27]   A. Gaffoor , D. Ravinder. *Characterization of Nano-Structured Nickel-Cobalt Ferrites Synthesized By Citrate-Gel Auto Combustion Method*, Journal Engineering Res. Applied, 4, 73 (2014).

[28]   A.A Thant, S. Srimala, P. Kaung, M. Itoh, Radzali and M.N.A. Fauzi, *Low temperature synthesis of MgFe2O4 soft ferrite nanocrystalline*, Journal of Australian Ceramic Society, 46, 11, (2010);

[29]   N. Kaur and M. Kaur. *Comparative studies on impact of synthesis methods on structural and magnetic properties of magnesium ferrite nanoparticles* Processing and Application of Ceramics 8, 137 (2014); https://doi.org/10.2298/PAC1403137K.

[30]   N. Sivakumara, A. Narayanasamya, J.M. Greneche, R. Murugaraj, Y.S, Leed. *Electrical and magnetic behaviour of nanostructured MgFe$_2$O$_4$ spinel ferrite*, journal of alloys and compound, 504, 395 (2010); https://doi.org/10.1016/j.jallcom.2010.05.125.

[31]   K.B. Modi, M.K. Rangolia, M.C. Chhantbar and H.H. Joshi, *Study of infrared spectroscopy and elastic properties of fine and coarse grained nickel–cadmium ferrites*, Journal of Material Science,41, 7308 (2006); https://doi.org/10.1007/s10853-006-0929-3.

[32]   B.D. Cullity, Stock SR. *Elements of X-Ray diffraction*, 3rd ed. Hampshire (NJ), USA*: Prentice Hall.*167 (2006).

[33]   N. Farhana, H.K. Dubey, C. Verma, P. Lahiri, *Structural and magnetic properties of MgFe$_2$O$_4$ Nanopowder synthesized via co-precipitation route*,SN Applied Sci*ence, 2, 808, (2020);*https://doi.org/ 2611-9.

[34]   P.P. Hankare, V.T. Vader, N.M. Patil, SDJB Sankpal, M.R. Kadam, B.K. Chougule, N.S. Gajbhiye. *Synthesis, characterization and studies on magnetic and electrical propertiesof Mg ferrite with Cr substitution,* Material Chemistry Phy*sics,* 113, 233 (2009); https://doi.org/10.1016/j.matchemphys.2008.07.066.

[35]   A.T. Pathan, S.N. Mathad and A.M. Shaikh. *Infrared spectral studies of nanostructured Co^{2+} substituted Li- Ni Zn ferrites*, International Journal Self-Prop High Temp Synthesis, 3, 112 (2014);https://doi.org/10.3103/S1061386214020083.

[36]   E.D. Case, J.R. Smyth, V. Monthei. *Grain size determinations*, Journal American Ceramic Society, 64 24(1981).

[37]   R. Gupta, A.K. Sood, P. Metcalf and J.M. Honig, *Raman study of stoichiometric and Zn-doped Fe$_3$O$_4$,* Physics Review, B 65, 1 (2002); https://doi.org/10.1103/PhysRevB.65.104430.

[38]   L.V. Gasparov and D.B. Tanner*, Infrared and Raman studies of the Verwey transition in magnetite,* Journal American Physics, Society, 62 1-7, (1999); https://doi.org/10.1103/PhysRevB.62.7939.

[39]   G.V.M. Jacintho, A.G. Brolo, P. Corio, P.A.Z. Suarez and J.C. Rubim, *Structural Investigation of MFe$_2$O$_4$ (M= Fe,Co) Magnetic Fluids,J. Phys. Chem.* 113, 7684 (2009); https://doi.org/10.1021/jp9013477.

[40]   Z. Wang , P. Lazor , S.K. Saxena and HSC Neill, *High pressure Raman spectroscopy of ferrite MgFe$_2$O$_4$,* Material research Bulletin, 37, 1589 (2002); https://doi.org/10.1016/S0025-5408(02)00819-X.

[41]   41. J. Chandradass, A.H. Jadhav, K.H. Kim and H. Kim, *Influence of processing methodology on the structural and magnetic behavior of MgFe$_2$O$_4$ nanopowders*, Journal of Alloys Compound, 517, 164 (2012); https://doi.org/10.1016/j.jallcom.2011.12.071.

[42]   V. Sepelak, I. Bergmann, D. Menzel, A. Feldhoff, P. Heitjans, F.J. Litterst and K.D. Becker. *Magnetization enhancement in nanosized MgFe2O4 prepared by mechanosynthesis,* Journal of Magnetism and Magnetic Materials, 316, 764 (2007); https://doi.org/10.1016/j.jmmm.2007.03.087.

[43]   Y. Huang, Y. Tang, J. Wang and Q. Chen, Synthesis of MgFe2O4 nanocrystallites under mild conditions. Material Chemistry Physics, 97, 394 (2006); https://doi.org/10.1016/j.matchemphys.2005.08.035.

[44]   M.M. Rashad, *Magnetic properties of nanocrystalline magnesium ferrite by co-precipitation assisted with ultrasound irradiation*, Journal Material Science, 42, 5248 (2007);https://doi.org/10.1007/s10853-006-0389-9.

[45]   B. Viswanathan, V.R.K. Murthy, *Ferrite Materials Science and Technology*. I ed., Toppan company(s) Pte. Ltd, Singapore. 2-16, (1990).

[46]   M.A. Gabal, M. Reda, R.M. El-Shishtawy and Y.M. Al Angari, *Structural and magnetic properties of nano-crystalline Ni- Zn ferrites synthesized using egg-white precursor,* Journal of Magnetism and Magnetic Materials324, 2258 (2012); https://doi.org/10.1016/j.jmmm.2012.02.112.

[47]   A.Pradeep, P. Priyadharsini, G. Chandrasekaran, *Sol–gel route of synthesis of nanoparticles of MgFe$_2$O$_4$ and XRD, FTIR and VSM study*, Journal of Magnetism and Magnetic Materials, 320, 2774 (2008);https://doi.org/10.1016/j.jmmm.2008.06.012.

[48]   Y. Ichiyanagi, M. Kubota, S. Moritake, Y. Kanazawa, T. Yamada and T. Uehash, *Magnetic properties of Mg Ferrite nanoparticles,* Journal of Magnetism and Magnetic Materials, 310, 2378 (2007); https://doi.org/10.1016/j.jmmm.2006.10.737.

[49] S. Rahman, K. Nadeem, M.A. Rehman, M. Mumtaz, S. Naeem, I.L. Papst, *Structural and magnetic properties of ZnMg-ferrite nanoparticles prepared using the co-precipitation method*, Ceramic International, 39, 5235 (2013); http://dx.doi.org/10.1016/j.ceramint.2012.12.023.

[50] 50. R.C. Kambale, P.A. Shaikh, C.H. Bhosale, K.Y. Rajpure, Y.D. Kolekar, *The effect of Mn substitution on the magnetic and dielectric properties of cobalt ferrite synthesized by an autocombustion*, Smart. Material Structure18, 1 (2009); https://doi.org/10.1088/0964- 1726/18/11/115028.

[51] S.K. Durrania, S. Naz, M. Mehmood, M. Nadeem and M. Siddique, *Structural, impedance and Mössbauer studies of Magnesium ferrite synthesized via sol-gel auto- combustion Process*, Journal Saudi Chemstry Society, 21, 1, (2017); https://doi.org/10.1016/j.jscs.2015.12.006.

[52] C. Kumari, H.K. Dubey, F. Naaz, P. Lahiri, *Structural and optical properties of nanosized Co substituted Ni ferrites by coprecipitation method,* Phase Transition, 93, 1 (2020); https://doi.org/10.1080/01411594.2019.1709120.

[53] G.D. Nipan, V.A. Ketsko, A.I. Stognij, A.V. Trukhanov, T.N. Koltsova, M.A. Kopeva, L.V. Elesina, N.T. Kuznetsov, *Properties of Mg(Fe$_{1-x}$Ga$_x$)$_2$O$_4$ Solid Solutions in Stable and Metastable States*, Inorganic Material, 46, 490 (2010);

[54] H.G. Kim, P.H. Borse, J.S. Jang, E.D. Jeong, O.S. Jung, Y.J. Suh, J.S. Lee, *Fabrication of CaFe$_2$O$_4$/MgFe$_2$O$_4$ bulk heterojunction for enhanced visible light photocatalysis* Chemistry Communication, 39, 5889 (2009).

[55] H. Xiang, X. Peng, D. Xu, X. Yang, G. Ren, Z. Zhang, Y. Zhong and X. Wang. *One-pot solvent-free synthesis of MgFe2O4 nanoparticles from ferrous sulfate waste*, Material and Manufacturing Processes, 35,590 (2020); https://doi.org/10.1016/j.mtcomm.2020.101516.

[56] V.K. Mittal, S. Bera, R. Nithya, M.P. Srinivasan, S. Velmurugan, S.V. Narasimhan, *Solid State Synthesis of Mg–Ni Ferrite and Characterization by XRD and XPS,* Journal Nuclear Material, 335, 302 (2004);http://dx.doi.org/10.1016%2Fj.jnucmat.2004.05.010.

Ф.Нааз[1], П. Лахірі[1*], Ч. Кумарі[1], Х. Кумар Дубей[2]

Спектроскопічні, магнітні та морфологічні дослідження нанопорошку MgFe₂O₄

[1]*Кафедра хімії, Інститут наук, ММВ, Університет Банараса Хінду, Ванарас-221005, Індія, plahiri16@yahoo.com*
[2]*Кафедра хімії, коледж BRDPG, Деорія-274001, Індія*

Нано феритову сполуку типу шпінелі MgFe₂O₄ синтезовано золь-гель методом із використанням нітратів металів як прекурсорів. Фазовий склад, морфологію та елементний аналіз фериту магнію (MgFe₂O₄) здійснено методами дифракції Х-променів, перетворення Фур'є в інфрачервоному діапазоні, атомно-силової мікроскопії, енергодисперсійної Х-променевої та скануючої електронної мікроскопії. Х-променева дифракційна картина зразка підтверджує існування однофазного матеріалу, для якого оцінка розмірів кристалітів склала 39,9 нм. Дослідження в інфрачервоному діапазоні із використанням перетворенням Фур'є підтвердило наявність коливань метал-кисень, що відповідають тетраедричним і октаедричним вузлам відповідно. Із результатів скануючої електронної мікроскопії отримано розмір зерене, який склав приблизно 97,7 нм. Спектри комбінаційного розсіювання зразка демонструють п'ять активних мод раманівського розсіювання (A₁g + Eg + 3F₂g), що сумісно зі структурою шпінелі. Дослідження магнітних характеристик при кімнатній температурі показує поведінку петлі гістерезису з низьким значенням намагніченості насичення, 27,192 emug⁻¹ і незначним значенням коерцитивної сили. Ширину забороненої зони визначено за допомогою спектрів пропускання в УФ-діапазону. Крім того, для підтвердження ступенів окислення та дослідження хімічного складу зразка використано методи рентгенівської фотоелектронної спектроскопії.

Ключові слова: феритова шпінель, нанокристали, дифракція Х-променів, спектри комбінаційного розсіювання, магнітні властивості.